buildings

MDPI

Article

Combined Impact of Nano-SiO_2 and Superabsorbent Polymers on Early-Age Concrete Engineering Properties for Water-Related Structures

Weiwei Zhang [1], Guo Yang [1,*], Wenrong Yun [2], Jinghao Li [3], Jun Xie [4], Wenbo Wu [1] and Zhixuan Deng [1]

[1] College of Civil and Transportation Engineering, Hohai University, Nanjing 210098, China; 13871140998@163.com (W.Z.); wuwb7155@163.com (W.W.); 231304020004@hhu.edu.cn (Z.D.)
[2] Wujin District River and Lake Management Office, Changzhou 213159, China; wjywr@163.com
[3] School of Civil Engineering, Chongqing University, Chongqing 400045, China; 18203040956@163.com
[4] Nanjing Electric Power Design and Research Institute Co., Ltd., Nanjing 210036, China; 15195929464@163.com
* Correspondence: yangguoneo@hotmail.com; Tel.: +86-18262638803

Abstract: High-performance concrete (HPC) is currently widely used in water-related structures. The incorporation of nano-silica (nano-SiO_2, NS) can further refine its pore structure, thereby enhancing the compressive strength and durability of HPC without necessitating a reduction in the water-to-binder (w/b) ratio. However, the addition of nano-materials significantly increases the autogenous shrinkage (AS) of concrete, leading to elevated tensile stresses and making the concrete more susceptible to early-age cracking. To mitigate AS, superabsorbent polymers (SAPs) can be introduced to internally cure the concrete, thereby improving the internal relative humidity (IRH) and reducing the AS in NS-reinforced concrete. In this study, we experimentally investigate the setting behavior, pore structure, compressive strength, IRH, and AS properties of concrete with a w/b of 0.3, incorporating both NS and SAP. The results demonstrate that the addition of NS advances setting time, significantly densifies the pore structure, markedly enhances compressive strength, accelerates the decline in IRH, and increases AS strain. Conversely, the incorporation of SAP exhibits opposite effects on these properties, particularly in substantially mitigating AS strain. The combined incorporation of 1.5% NS and 0.15% (or 0.30%) SAP achieves both higher compressive strength and lower AS strain compared to plain concrete at 28 days. These findings suggest that the simultaneous introduction of NS and SAPs into concrete formulations is recommended to achieve an optimal balance between shrinkage and strength properties. Such advancements are particularly beneficial for applications in hydraulic and water-related structures, where enhanced durability and reduced cracking are critical for maintaining structural integrity and ensuring longevity.

Keywords: hydraulic structures; nano-SiO_2; superabsorbent polymers; compressive strength; pore structure; autogenous shrinkage; early-age concrete

check for updates

Academic Editor: Vipul Patel

Received: 24 December 2024
Revised: 19 January 2025
Accepted: 22 January 2025
Published: 25 January 2025

Citation: Zhang, W.; Yang, G.; Yun, W.; Li, J.; Xie, J.; Wu, W.; Deng, Z. Combined Impact of Nano-SiO_2 and Superabsorbent Polymers on Early-Age Concrete Engineering Properties for Water-Related Structures. *Buildings* **2025**, *15*, 374. https://doi.org/10.3390/buildings15030374

Copyright: © 2025 by the authors. Licensee MDPI, Basel, Switzerland. This article is an open access article distributed under the terms and conditions of the Creative Commons Attribution (CC BY) license (https://creativecommons.org/licenses/by/4.0/).

1. Introduction

Concrete is a widely consumed material in civil engineering, prized for its excellent workability and durability [1–3]. As the field of civil engineering advances, the demand for concrete with higher strength and enhanced durability continues to grow [4], particularly for applications in long-span structures, high-rise buildings, and environments subjected to harsh conditions [5]. High-performance concrete (HPC) is the main design standard based on basic mechanical property requirements, with a high durability, high working capacity,

and high volume stability [6,7]. In the context of water-related structures—such as dams, bridges, water treatment facilities, and marine infrastructure—the mechanical properties and durability of concrete are critically important [7]. These attributes are intrinsically governed by the nano-level pore structure of the material. Nano-materials, therefore, present a promising avenue for refining the pore structure of concrete, thereby enhancing its compressive strength and overall durability [8–12]. In water-related structures, where concrete is often exposed to aggressive environments [3,13–15], improved pore refinement can lead to superior resistance against water-induced degradation, such as chloride ion penetration, sulfate attack, and freeze–thaw cycles. Consequently, the incorporation of nano-materials not only augments the structural integrity of concrete, but also extends its service life in aquatic and hydrostatic conditions.

Among nano-materials, nano-silica (nano-SiO_2, NS) exhibits outstanding performance, and is the most extensively utilized additive for enhancing the compressive strength and durability of concrete. Ganesh et al. investigated the influence of NS particles on the compressive strength of early-age, high-strength concrete, reporting that the 28-day compressive strengths increased from 50.1 MPa (0% NS), to 54.0 MPa (1% NS) and 59.0 MPa (2% NS) [5]. Similarly, Jo et al. [16] corroborated these findings, observing comparable improvements in compressive strength with NS incorporation. Furthermore, Said et al. [17] and Oltulu et al. [18] explored the impact of NS particles on the pore structure of cementitious materials, demonstrating that NS incorporation refines the pore structure, thereby enhancing mechanical properties and durability.

However, Chen et al. [19] and Quercia et al. [20] reported that the addition of NS leads to an increase in autogenous shrinkage (AS) strain in concrete. Excessive AS induces high tensile stresses under restrained conditions, potentially surpassing the tensile strength of concrete and resulting in early-age cracking [21,22]. Such cracking can significantly compromise the compressive strength and durability of concrete structures [23–27], which is particularly critical for water-related applications, such as dams, bridges, water treatment facilities, and marine infrastructures, where structural integrity is paramount. These detrimental effects are most pronounced at early ages, when the tensile strength of concrete is still developing. In addition, excessive AS will lead to long-term volume shrinkage deformation of the concrete structure, so that the structure size changes significantly [28]. Early cracks will be further expanded and connected in the process of long-term use, forming more serious structural cracks and destroying the integrity of the structure. Therefore, mitigating AS in NS-enhanced concrete during the early stages is essential for controlling shrinkage-induced cracking and ensuring the long-term performance and reliability of concrete in water-exposed environments [29].

AS refers to the humidity-induced deformation that is closely related to the moisture content within concrete. AS in concrete is primarily caused by internal chemical and physical processes during cement hydration. To introduce additional water into concrete, two curing methods are commonly employed: external curing and internal curing. External curing proves ineffective for HPC due to its dense pore structure, which is a result of a low water-to-binder ratio (w/b). Consequently, the internal curing (IC) method has been adopted to mitigate AS in HPC [30,31]. Currently, superabsorbent polymers (SAPs) are widely utilized as IC agents [32]. SAPs are covalently cross-linked polymers [33] that are capable of absorbing substantial amounts of water, thereby enhancing IC efficacy [34] and improving internal relative humidity (IRH). Qin et al. [35] proved that SAPs can effectively reduce the water-to-cement ratio, improving the density of the structure and thus significantly reducing the shrinkage of concrete, while having no adverse effects on the strength of concrete and improving the durability of concrete. However, studies by Shen et al. [36] and Canulpolanco et al. [37] have demonstrated a significant reduction in AS of

early-age concrete with increasing SAP content. However, the voids left after SAPs release the pre-absorbed water in HPC can deteriorate its pore structure, mechanical properties, and durability [38], which limits the adoption of the IC method in HPC [39].

Nevertheless, considering the synergistic mechanisms of NS and SAPs discussed previously, the adverse effects of SAPs on HPC can potentially be offset by incorporating NS, and vice versa. This synergy is expected to achieve an optimal balance between shrinkage control and strength enhancement. Despite this promising interaction, there is currently no systematic research investigating the combined influence of NS and SAPs on the pore structure, compressive strength, IRH, and AS properties of concrete. Addressing this gap, the present study experimentally investigates the setting behavior, pore structure, compressive strength, IRH, and AS properties of early-age concrete incorporating both NS and SAP, with a particular focus on applications in water-related structures. This research aims to provide comprehensive insights into optimizing concrete performance for hydraulic and water-exposed environments, thereby enhancing the structural integrity and longevity of critical water-related infrastructure.

2. Materials and Methods

2.1. Materials

Ordinary cement P. II 52.5 (with a density of 3180 kg/m^3 and a specific surface area of 380 m^2/kg), complying with China National Standard GB 175-2023 [40], was used. Table 1 lists the chemical compositions of the cement used. River sand (with a maximum size of 2.5 mm and a fineness modulus of 2.78) and crushed sandstone (with a continuous size distribution of 5–30 mm and an apparent density of 2600 kg/m^3) were employed as the fine and coarse aggregates, respectively.

Table 1. The chemical composition of the cement.

Component (wt%)	SiO_2	Al_2O_3	Fe_2O_3	CaO	MgO	Na_2O	K_2O	SO_3	TiO_2	LOI
Proportion	19.53	4.31	2.89	63.84	1.25	0.13	0.64	3.25	0.26	3.00

The nano-particles used were NS with an average particle size of 20 nm, a density of 0.4 g/cm^3, and a purity of 99% (see Figure 1a). The SAP used was provided by Jiangsu Subot Company, as shown in Figure 1b. The water absorption ability, tested by the tea-bag method [41] on the SAP at 24 h in pure water, was 14 g of water/g of SAP. A liquid polycarboxylic-based superplasticizer was applied to adjust the workability of the concrete. The water used in the test was tap water.



(**a**) (**b**)

Figure 1. The additive used in the experiment: (**a**) NS powder; (**b**) SAP powder.

2.2. Mix Proportions

For a given unit volume of concrete, the SAP mass needed was given as Equation (1) [42]:

$$M_{SAP} = \frac{C \cdot CS \cdot \alpha_{max}}{S \cdot \varphi_{SAP}} \quad (1)$$

where M_{SAP} is the dry SAP mass, kg/m^3; C_f is the cement content, kg/m^3; CS is the chemical shrinkage in the completely hydrated concrete, and is 0.06 g water/g cement in this study; α_{max} is the maximum hydration degree in theory, and is approximately (w/b)/0.36 when the w/b is below 0.36; S is the theoretical saturation degree of the SAP (0–1), and is taken to be 1; and φ_{SAP} is the water absorption capacity of the SAP.

As calculated by Equation (1), the dry SAP mass was 2.22 kg/m^3 and the IC water content was 31.09 kg/m^3. This article adopts the internal mixing method to ensure a constant quality of cementitious materials, which is beneficial for improving the strength and uniformity of concrete. A gradient SAP content was designed as 0, 0.80, and 1.60 kg/m^3, replacing 0, 0.15%, and 0.30% of the cement by mass, and the corresponding IC water contents were 0, 11.2, and 22.4 kg/m^3, respectively. According to the results of Khaloo et al. [43], a low NS content of 1.5% and 3.0% by mass of cement was utilized. The mix proportions of the concrete are listed in Table 2. The w/b of all the samples was 0.30. WC030 represents the concrete without NS and SAP incorporation (the reference sample). NS1.5S0.15 represents the concrete with a 1.5% content of NS and a 0.15% content of SAP. The average results of three samples in one proportion were taken as the final test data. The same processing method was performed for all the tests.

Table 2. The mix proportions of the concrete.

Mix Design	Compositions (%)		Mass of Components (kg/m^3)					
	NS	SAP	Cement	NS	Water	SAP	Sand	
gravelWC030	0	0	533.00	0	160	0	597	1110
NS1.5	1.5	0	525.01	7.99	160	0	597	1110
NS3.0	3.0	0	517.01	15.99	160	0	597	1110
NS1.5S0.15	1.5	0.15	524.21	7.99	160	0.80	597	1110
NS1.5S0.30	1.5	0.30	523.41	7.99	160	1.60	597	1110

2.3. Test Methods

2.3.1. Autogenous Shrinkage

Figure 2 exhibits the free deformation test setup. The samples were cast into a 100 mm × 100 mm × 515 mm prism shape by a steel prismatic mold. Two sensor supports were fixed on the top of the steel prismatic mold. Two eddy-current displacement sensors (ECDSs) were installed on the sensor supports. The position of the ECDSs should be previously adjusted for accurate testing. Two target seats, the distance between which should be not less than 400 mm, were fixed on the proper position on the steel prismatic mold bottom. Round holes were set in the two target seats to ensure the target seats were anchored well on the concrete and ensure deformation consistency between the concrete and the standard target. The standard targets were magnetically attached to the target seats.

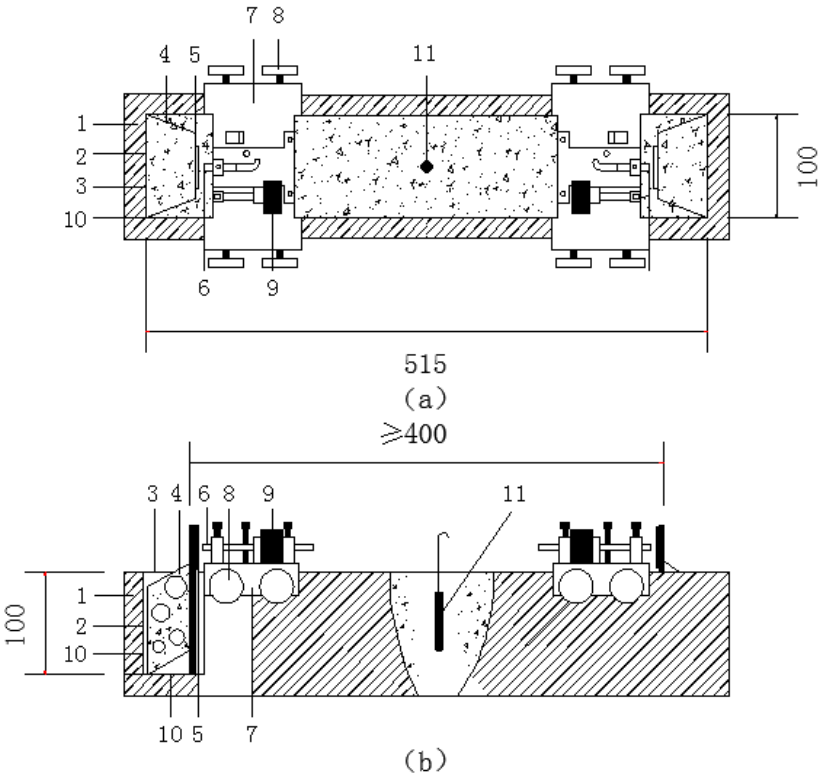


Figure 2. AS and temperature test setup layout: (**a**) top view; (**b**) front view. 1. Steel prismatic mold; 2. Polyethylene film; 3. Concrete; 4. Target seat; 5. Standard target; 6. ECDS; 7. Sensor support; 8. Fastening bolt; 9. Fitting screw; 10. Teflon sheet; 11. Temperature sensor.

The preparation of sample mixtures for the investigation of setting time, compressive strength, IRH, and AS followed the same mixing procedure as prescribed in ASTM C192-06/C192M-16 [44]. Before the test, the NS powder (and dry SAP powder) was mixed thoroughly with cement to make the binder materials. Then, the aggregates, binder materials, water, and superplasticizer were put into the mixer in turn and mixed evenly. During casting, a temperature sensor with an accuracy of 0.1 °C was embedded in the center of the steel prismatic mold to monitor the temperature change. After casting, the target seats should be embedded in the concrete so that they are simultaneously moved with the concrete. The internal and bottom walls of the steel prismatic mold were covered with a layer of Teflon sheet and a layer of polyethylene sheet to minimize friction. The top surface of the sample was sealed with two layers of polyethylene sheets [45]. The standard targets and the ECDSs fixed on them composed the eddy-current stirring-up components; the electric signals measured by these were converted by the signal transformer into displacement signals. The data were acquired every 15 min and lasted for 28 days. Finally, the samples were cured in a room with a temperature of 20 ± 2 °C and a relative humidity (RH) greater than 95%.

The initial setting time (IST) was set as the AS starting point [46]. The free deformation measured contained the thermal deformation due to the cement hydration [47]. The AS strain was isolated from the free deformation using Equation (2):

$$\varepsilon_{AS}(t) = \varepsilon_{free}(t) - \alpha(t) \cdot [T(t) - T_0] \quad (2)$$

where $\varepsilon_{AS}(t)$ is the AS strain, με; $\varepsilon_{free}(t)$ is the free deformation strain, με; $\alpha(t)$ is the thermal expansion coefficient (CTE), με/°C; $T(t)$ is the concrete temperature, °C; T_0 is the initial temperature, °C; and t is the age since AS starting point, days.

The CTE varied with age, and was calculated according to Equation (3) [48]:

$$\alpha_T(t) = \alpha_{28} \times \left(1 + 41 \times (t \cdot 24)^{-m}\right) \quad (3)$$

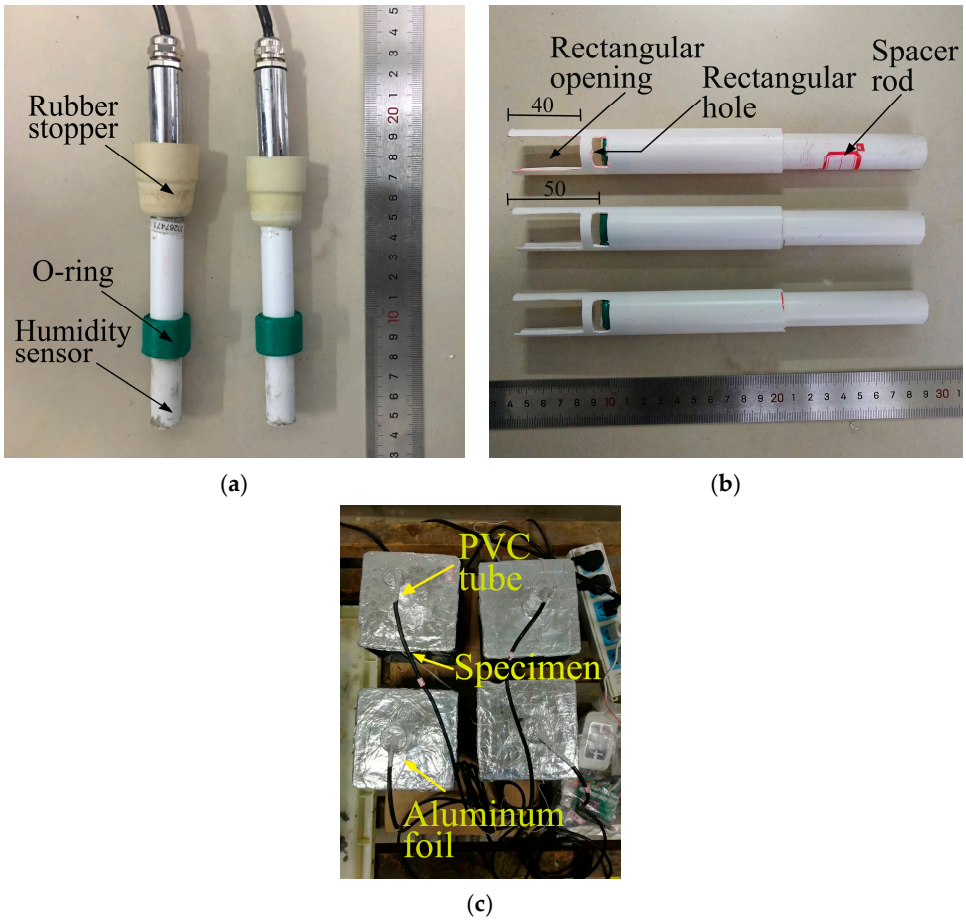
where α_{28} is the CTE at day 28, and is 8 $\mu\varepsilon/°C$; and m is an experimental constant, and equals 2.0.

2.3.2. Setting Behavior

The setting behavior was monitored by the capillary pressure method [49]. The negative capillary pressure test involves measuring the imbalance of water potential in the capillary and the change in negative capillary pressure in the process of rebalancing [50–52]. The samples for investigating setting times were sealed on the top by plastic film and subjected to the same curing conditions as for the AS samples.

2.3.3. Internal Relative Humidity

The 28-day-long IRH was measured for the 100 mm-long cubic sample using a HC2A-S (Rotronic) humidity sensor whose diameter was 15 mm, measurement range was from 1% to 100% RH, and accuracy was ±0.8% RH (see Figure 3a). Prior to and post-testing, the humidity sensors should be calibrated in a specific RH environment at 20 °C; for this, saturated NaCl (75.5% RH), KBr (81.7% RH), KCl (85.1% RH), and K_2SO_4 (97.6% RH) solutions may be used [53].



(**a**) (**b**)

(**c**)

Figure 3. Humidity test setup: (**a**) humidity sensor; (**b**) PVC tube and spacer rod; (**c**) humidity sample.

Figure 3b presents the PVC tube prepared to place and locate the humidity sensor. Rectangular openings and rectangular holes were set on the PVC tube to ensure that the

humidity sensor could sense the moisture exchange of the concrete. The middle of the rectangular hole was set as the measurement point. The space of the PVC tube above the measurement end of the humidity sensor was isolated by an O-ring. A rubber stopper, with the center perforated, was fixed on the top of the humidity sensor. To avoid moisture loss, three layers of plastic film were covered on the inner surfaces of the mold.

The PVC tube should be placed into and brought into contact with the bottom of the mold before casting, and should always be maintained vertically. A rubber bar, as a spacer rod, was pre-inserted into the PVC tube up to the measurement point, to preserve the space of the humidity sensor. After compacting, the sample was immediately covered by three layers of plastic film, and then cured with the AS samples. The spacer rod was replaced with the humidity sensor after the initial set. To prevent condensation on the humidity sensor, the humidity sensor underwent several cycles of being pulled out, cleaned, and inserted every 10 min or even less at first, then began automatic measurement when the humidity value was less than 100%. Then, the top of the PVC tube was sealed with a rubber stopper, the sample top was sealed with aluminum foil, and the gap was smeared with Vaseline.

2.3.4. Compressive Strength

The compressive strength of the concrete was tested on the 150 mm long cubic samples according to ASTM C39/C39M-20 [46]. All the samples were poured out from the mold at 24 h after casting, and cured to the test ages of 3, 7, 14, and 28 days.

2.3.5. Pore Structure

The pore structure of the mortar, based on its pore size distribution (PSD) and porosity, was determined using a low-field nuclear magnetic resonance (LF-NMR) method, as described in reference [54]. The curing temperature was kept constant, at 20 °C.

3. Results and Discussion

3.1. Setting Behavior

The setting time results are depicted in Figure 4. A larger NS additive content produced a shorter setting time, which indicated that the introduction of NS could advance the concrete setting process. Compared with WC030, when the NS content increased from 0 to 3.0%, the IST (FST) was shortened by 31.90% (15.38%). NS incorporation accelerates cement hydration [55], contributing to the development of the cementitious skeleton, which leads to an earlier setting behavior [56]. Meanwhile, longer setting times were obtained with the addition of a higher SAP content, which meant that SAP incorporation retarded the concrete setting process. The 0.30% SAP incorporation increased the IST (FST) of NS1.5 by 15.61% (9.91%). Zheng et al. [57] stated that saturation behavior of portlandite was closely related to the cement hydration, which governed the setting behavior. Cement hydration requires the participation of water, and appropriate saturation can ensure the full contact of cement particles with water, so as to accelerate the hydration reaction. If the saturation of portlandite is too high or too low, this will influence the cement setting time. Therefore, the setting behavior of portlandite can be determined by its saturation behavior. The water released from SAPs during IC delays the saturation of portlandite, which results in the retardation of concrete setting [58].

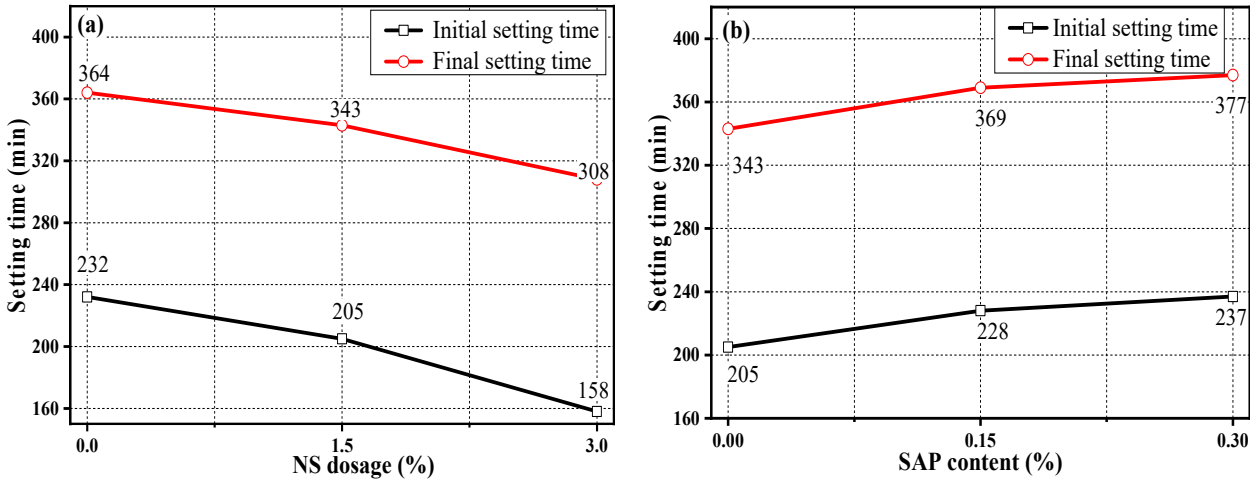


Figure 4. Setting time: (**a**) concrete containing NS; (**b**) concrete containing NS and SAP.

3.2. Pore Structure

The pore structure results, according to PSD, most probable pore diameter (MPPD), and porosity, are presented in Figure 5. Note that the pores with a diameter of 5–50 nm have a significant impact on AS strain development, because AS strain mainly occurs in such regions, while the porosity greatly affects mechanical strength [59]; this will be discussed in detail in the following sections.

As the NS content increases, it can be observed that the PSD curve of WC035 moves towards the smaller pore size region, which is verified by the decrease in MPPD, and the porosity decreases, implying that the pore structure was refined and densified with increasing NS addition. The MPPD and porosity at 28 days of NS1.5 (NS3.0) are 13.0% (18.8%) and 9.4% (14.9%), which are lower than those of WC035. On the one hand, the NS particles fill the gaps between the cement particles and the voids in the hydration products, making the pore structure denser on the physical level; on the other hand, owing to the extremely fine particles and large specific surface area of NS particles, the NS particles work as nucleation sites, accelerating the nucleation of C-S-H gel on the surface of the NS particles and advancing cement hydration, which compacts the pore structure on the surface chemistry level [60,61]. In addition, the cement hydration process is further accelerated, and much C-S-H gel is formed, owing to the pozzolanic reaction between the NS particles and portlandite, which contributes to a denser pore structure on the chemical level [62]. Together, these three aspects contribute to establishing a dense, uniform, and solid pore structure.

SAP incorporation had an opposite effect on pore structure compared with that of NS incorporation. With increasing SAP addition, the PSD curve of NS1.5 shifts towards the larger pore size region, which is proved by the increase in MPPD, and porosity increases, indicating that SAP incorporation loosened and weakened the pore structure. An SAP addition of 0.15% (0.30%) led to a 32.0% (62.6%) and 3.8% (8.4%) rise in the MPPD and porosity of NS1.5, respectively. This is attributed to the fact that, on the one hand, the SAP desorbs the IC water, contributing to cement hydration [63], which can be considered a positive effect, as discussed above; on the other hand, the voids left after the SAP desorbs the IC water loosen the pore structure, which can be considered a negative effect. When the negative effect is superior to the positive effect, the pore structure becomes loose, which is proved by the test results.

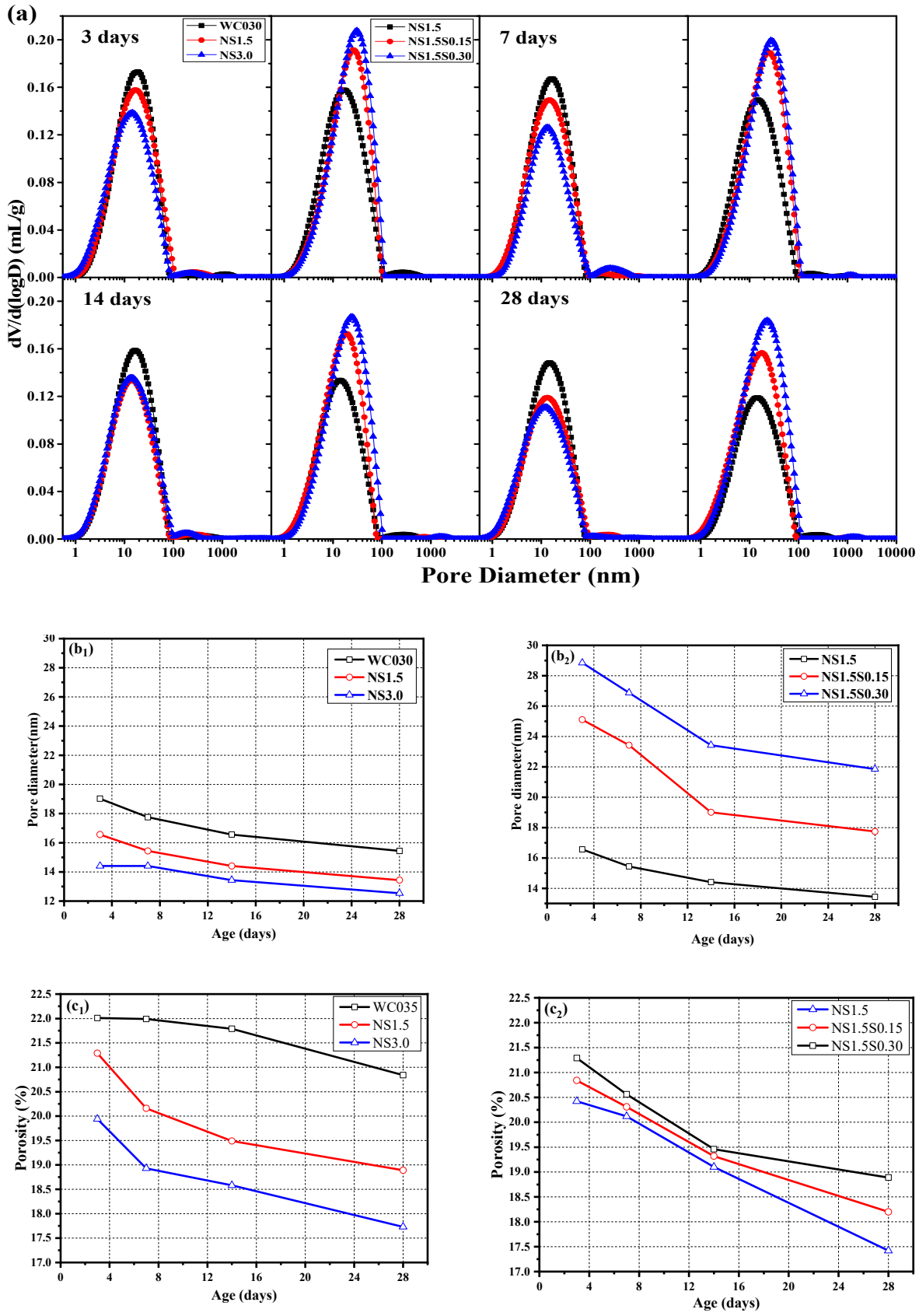


Figure 5. Pore structure of concrete with incorporation of NS and SAP at 3, 7, 14, and 28 days: (**a**) PSD; (**b**$_1$,**b**$_2$) MPPD; (**c**$_1$,**c**$_2$) porosity.

3.3. Compressive Strength

The compressive strength results are given in Figure 6. The compressive strength became enhanced with age and increased NS content. The 3-day compressive strengths of NS1.5 and NS3.0 were 108.78% and 118.46% of that of WC030, respectively. This strength reinforcement effect increased to a maximum of 22.82% and 32.74% at 14 days, and then decreased to 6.68% and 14.90% at 28 days, respectively. This is mainly because a lower porosity was obtained with the incorporation of a higher NS content (see Figure 5), which meant that there were fewer inner micro-defects, and hence the mechanical strength was stronger. The cement hydrated at a fast rate at an early age, and then at a slow rate, especially under the acceleration effect of NS, which determined the enhancement rate of compressive strength.

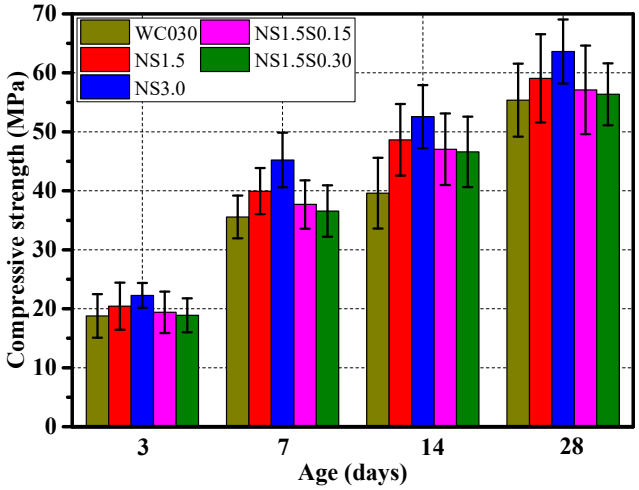


Figure 6. Compressive strengths of concrete with incorporation of NS and SAP.

In contrast to the effect of NS on compressive strength, SAP incorporation had a weakening effect on compressive strength, which intensified with increased SAP content. However, the decrease in the strength of the NS concrete induced by the addition of SAP decreased with age. SAP incorporations of 0.15% and 0.30% led to a 5.13% and 7.58% reduction in the 3-day compressive strength of NS1.5, respectively. These strength declines were reduced to 3.30% and 4.57% at 28 days, respectively. The introduction of SAP could deteriorate the pore structure, evidenced by increasing porosity (see Figure 5), which would weaken the mechanical strength. The water desorption rate of SAPs decreases with age [64]; therefore, most of the absorbent water was released at an early age, which accounts for the fact that the loss of strength due to SAP incorporation decreased with age. However, the compressive strengths of concrete with the combined incorporation of NS and SAP were stronger than those of the reference sample. The increment in the 28-day compressive strength of WC030 was 3.16% (1.81%), due to 1.5% NS and 0.15% (0.30%) SAP incorporation.

3.4. Internal Relative Humidity

The IRH results are depicted in Figure 7. The IRH of all the samples remained saturated for some time, and then declined with age [43]. NS and SAP incorporation obviously affected the IRH properties of the concrete.

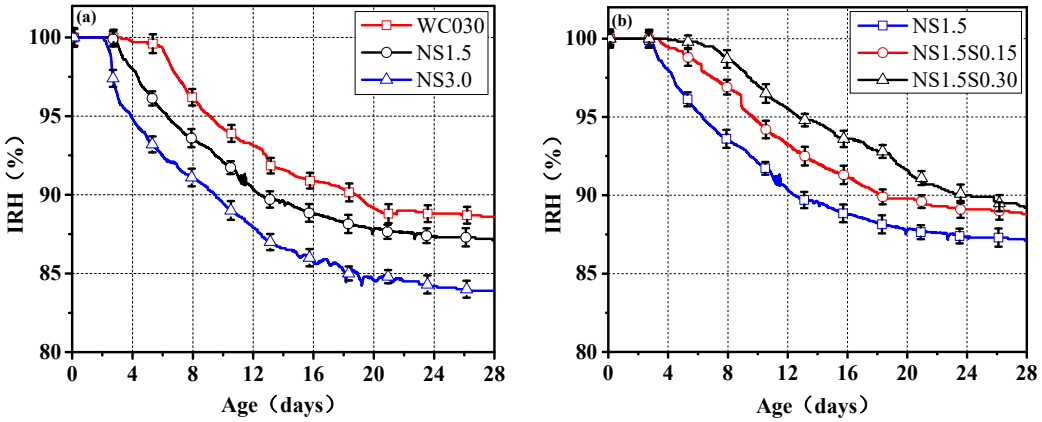


Figure 7. IRH of concrete with the incorporation of NS and SAP: (**a**) NS; (**b**) NS and SAP.

NS introduction shortened the saturation period, which intensified with the addition of NS. The critical times, which equal the saturation periods, of NS1.5 and NS3.0 were 15.9 and 27.8 h shorter than that of the reference sample, respectively. During the unsaturation period, the IRH decreased gradually with increasing NS content. The 28-day IRHs of WC030, NS1.5, and NS3.0 were 88.6%, 87.1%, and 83.9%, respectively. The water in capillary pores is consumed during cement hydration; therefore, the amount of moisture left decreased with age, characterized by a drop in IRH. NS incorporation accelerates cement hydration as discussed above, leading to faster water consumption and subsequently a more rapid self-desiccation and decline in IRH compared with the reference sample; as such, this mechanism intensified with increasing NS content.

SAP incorporation had an opposite effect on IRH compared with NS incorporation. The saturation period of concrete was prolonged by SAP incorporation, and increased with increasing SAP content. The critical times of NS1.5S0.15 and NS1.50.30 were 19.3 and 33.8 h longer than that of NS1.5, respectively. During the unsaturation period, SAP introduction improved the IRH performance of concrete with NS incorporation, featuring a slower IRH decline induced by the introduction of a higher SAP content. The 28-day IRHs of NS1.5S0.15 and NS1.50.30 were 1.7% and 2.1% higher than that of NS1.5, respectively. Such phenomena are related to the water desorption behavior of SAPs. When cement hydration consumes the water in capillary pores, a meniscus forms and capillary pore pressure occurs, which forces SAPs to release the pre-absorbed water, alleviating water consumption and delaying the development of self-desiccation and decline in IRH.

3.5. Autogenous Shrinkage

3.5.1. AS of Concrete with NS Incorporation

The AS strain results are presented in Figure 8. The AS property can be divided into two stages, i.e., the AS strain increased rapidly and sharply during the first 4 days, especially the first 2 days, and then increased slowly, at a gradually decreasing rate. More than 12% and 30% of 28-day AS strain had been reached within about 2 and 4 days for all the samples, respectively.

A particularly significant AS strain was exhibited by the reference sample because of large self-desiccation due to the low w/b of the reference sample [65]. NS incorporation had a significant influence on the AS strain of the concrete, that is, the AS strain evidently increased with increasing NS content, especially at early age. With the introduction of 1.5% and 3.0% NS, the 28-day AS strain of WC035 increased by 37.87% and 75.74%, respectively. This is because NS particles accelerate cement hydration, refine the pore structure (see Figure 5), and quicken the decline in IRH (see Figure 7) and self-desiccation, as described above, which generates a higher capillary pressure on the pore walls, and therefore induced

a higher AS compared with the reference sample. This mechanism becomes intense with increasing NS content.

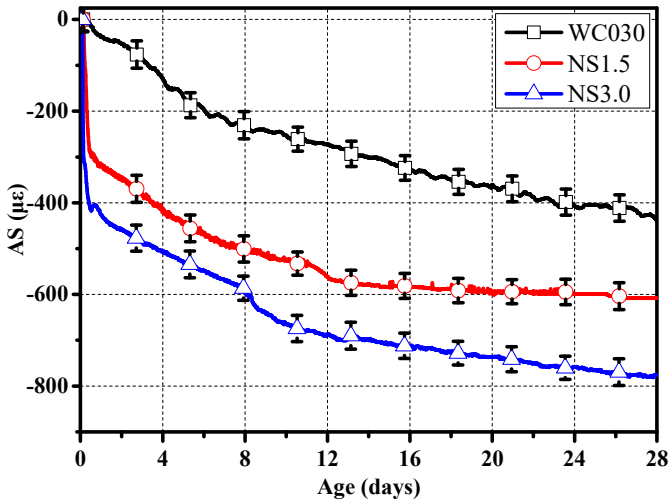


Figure 8. AS of concrete containing NS.

Apart from AS strain itself, the shrinkage development rate is also important for shrinkage stress development and early-age crack control, because the tensile strength and creep-induced relaxation effect can develop sufficiently to allow the concrete to resist cracks when the shrinkage rate is low. The AS development rate of concrete can be calculated according to Equation (4) [66]:

$$R(t) = \frac{d\varepsilon_{AS}(t)}{dt} \quad (4)$$

where $R(t)$ is the AS development rate of concrete at t days, με/days.

Figure 9 gives the AS development rates of the reference sample, along with the concrete incorporating NS. The positive value represents the shrinkage rate. The AS rates for all the samples began higher, decreased sharply during the first 4 days, then decreased slowly until 20 days, and subsequently stabilized. The AS rates of the reference sample increased gradually with increasing NS content. On day 1, the AS rate of WC030 increased by 316.0% due to a 3.0% NS addition. Hence, NS incorporation leads to an adverse effect on cracking control.

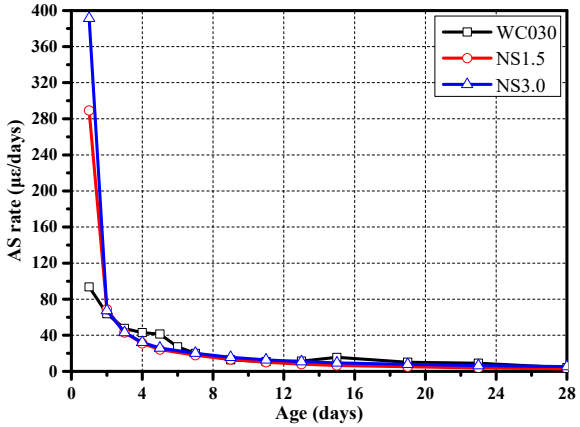


Figure 9. AS development rate of concrete containing NS.

3.5.2. AS of Concrete with Combined Incorporation of NS and SAP

The AS results of concrete incorporating NS and SAP are exhibited in Figure 10. The AS development trend of concrete with the combined incorporation of NS and SAP was

similar to that of concrete with NS incorporation only. SAP incorporation contributed to mitigating the AS strain of NS concrete, which intensified with increasing SAP content. SAP incorporation of 0.15% and 0.30% achieved a 35.86% and 49.84% reduction in the 28-day AS of NS1.5, respectively. As previously mentioned, this is because SAP introduction deteriorates the pore structure (see Figure 5) and maintains the IRH at a higher level (see Figure 7), which delays self-desiccation, inhibits an increase in capillary pore pressure, and mitigates AS strain. Therefore, the higher the SAP content, the higher the IC efficacy of SAP, and the better the concrete's AS property.

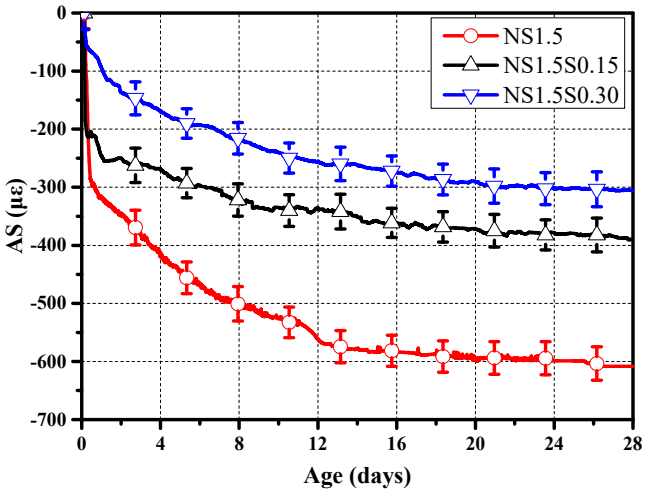


Figure 10. AS of concrete with combined incorporation of NS and SAP.

Figure 11 shows the AS development rates of concrete with the combined incorporation NS and SAP. Similar regularity was shared by the trends in the AS development rate of concrete with combined NS and SAP incorporation and those of concrete containing NS only. The AS development rate of NS concrete decreased gradually with increasing SAP content during the first 2 days. An SAP incorporation of 0.30% decreased the AS development rate of NS1.5 by 68.5%. Therefore, the introduction of SAPs into NS-reinforced concrete is greatly beneficial to shrinkage cracking control.

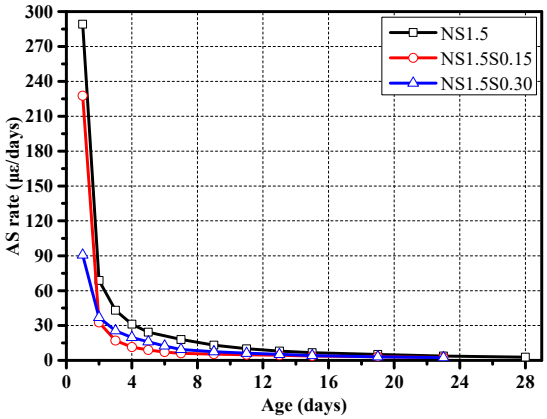


Figure 11. AS rate of concrete with combined use of NS and SAP.

Based on the obtained macroscopic properties results (compressive strength and AS strain), the combined incorporation of NS and SAP has the potential to produce advanced concrete with better comprehensive properties than plain concrete. The 28-day compressive strength and AS strain of the reference sample increased by 4.84% (3.05%) and −11.56% (−30.84%) due to 1.5% NS and 0.15% (0.30%) SAP incorporation, respectively, indicating

that a good strength-shrinkage property of concrete can be achieved by the simultaneous use of NS and SAP, as expected. The optimal mixing ratio of NS and SAP in early-age concrete still needs further investigation.

4. Conclusions

The main conclusions drawn from this paper are as follows:

(1) NS incorporation accelerated the setting time of concrete, significantly improving its pore structure by densifying the PSD, decreasing the MPPD, and reducing porosity, as well as decreasing the setting time, with the IST (FST) decreasing by 31.90% (15.38%) when the NS content was increased from 0 to 3.0% compared to WC030. Conversely, SAP incorporation delayed the setting time and deteriorated the pore structure by counteracting the effects of NS. With an increase in SAP content, the condensation time increased, and 0.30% SAP incorporation increased the IST (FST) of NS1.5 by 15.61% (9.91%).

(2) NS incorporation greatly enhanced the compressive strength of concrete, while SAP introduction weakened its compressive strength. However, the combined incorporation of 1.5% NS and 0.15% (or 0.30%) of SAP enhanced the compressive strength by 3.16% (1.81%) compared with the reference sample, demonstrating a synergistic effect that is beneficial for the structural integrity of water-related concrete applications.

(3) NS incorporation accelerated self-desiccation by shortening the saturation period and quickening the decline in IRH, which is critical for maintaining the material's properties over time. On the other hand, SAP significantly improved the IRH by counteracting the water loss caused by NS, with the 28-day IRHs of NS1.5S0.15 and NS1.50.30 being 1.7% and 2.1% higher than that of NS1.5, respectively. This is particularly advantageous for concrete in water-exposed environments, where maintaining adequate moisture levels during curing is essential for preventing shrinkage and cracking.

(4) NS incorporation increased the AS strain, but the IC efficacy of SAP effectively inhibited the development of AS strain, as well as the AS development rate. The combined incorporation of NS and SAP reduced the AS strain more effectively than the reference sample, enhancing with increasing SAP content, with 0.15% and 0.30% SAP incorporation reducing the 28-day AS of NS1.5 by 35.86% and 49.84%, respectively. This is crucial for the long-term durability and reliability of water-related concrete structures subjected to variable moisture conditions.

Author Contributions: Conceptualization, W.Z., G.Y., W.Y., J.L., and J.X.; data curation, Z.D.; formal analysis, W.Z., W.W., and Z.D.; funding acquisition, G.Y. and J.X.; investigation, W.Z.; methodology, W.Z., G.Y., and J.L.; project administration, G.Y. and J.X.; resources, W.W.; supervision, G.Y.; validation, W.Z., W.Y., and J.X.; writing—original draft, W.Z.; writing—review and editing, G.Y., W.Y., J.L., and J.X. All authors have read and agreed to the published version of the manuscript.

Funding: This research was funded by the Guangxi Science and Technology Program, under Grant (Guike AA23062034); the Fundamental Research Funds for the Central Universities (B240201179); the Natural Science Foundation of Jiangsu Province (BK20241532); the Technology Project of State Grid Jiangsu Electric Power Co., Ltd. (J2023094); and the Research on Key Technologies for Improving the Quality and Safety Assurance of the Huai River to Sea Waterway Phase II Project (RHSD2/FW-2024-03).

Data Availability Statement: The data used to support the findings of this study are available from the corresponding author upon request.

Conflicts of Interest: Author Wenrong Yun was employed by the company Wujin District River and Lake Management Office. Author Jun Xie was employed by the company Nanjing Electric Power Design and Research Institute Co., Ltd. The remaining authors declare that the research was conducted in the

absence of any commercial or financial relationships that could be construed as a potential conflict of interest. The authors declare that this study received funding from the Technology Project of State Grid Jiangsu Electric Power Co., Ltd. The funder was not involved in the study design, collection, analysis, interpretation of data, the writing of this article or the decision to submit it for publication.

References

1. Hou, D.; Li, T.; Wang, P. Molecular dynamics study on the structure and dynamics of NaCl solution transport in the nanometer channel of CASH gel. *ACS Sustain. Chem. Eng.* **2018**, *6*, 9498–9509. [CrossRef]
2. Zhang, X.X.; Gao, M.Q.; Pel, L.; Smeulders, D. An NMR study of the role of coir fibers in the hydration and drying of cement paste at early age. *J. Build. Eng.* **2023**, *71*, 106445. [CrossRef]
3. Li, Y.; Zhao, H.; Wei, Y.; Bao, T.; Li, T.; Wang, Q.; Wang, N.; Zhao, M. Vision-guided crack identification and size quantification framework for dam underwater concrete structures. *Struct. Health Monit.* **2024**, *24*, 14759217241287906. [CrossRef]
4. Lura, P.; Jensen, O.M.; Weiss, J. Cracking in cement paste induced by autogenous shrinkage. *Mater. Struct.* **2009**, *42*, 1089–1099. [CrossRef]
5. Ganesh, P.; Ramachandra Murthy, A.; Sundar Kumar, S.; Mohammed Saffiq Reheman, M.; Iyer, N.R. Effect of nanosilica on durability and mechanical properties of high-strength concrete. *Mag. Concr. Res.* **2016**, *68*, 229–236. [CrossRef]
6. Bharatkumar, B.H.; Narayanan, R.; Raghuprasad, B.K.; Ramachandramurthy, D.S. Mix proportioning of high performance concrete. *Cem. Constr. Comp.* **2001**, *23*, 71–80. [CrossRef]
7. Dushimimana, A.; Niyonsenga, A.A.; Nzamurambaho, F. A review on strength development of high performance concrete. *Constr. Build. Mater.* **2021**, *307*, 124865. [CrossRef]
8. Li, Y.; Bao, T.; Huang, X.; Chen, H.; Xu, B.; Shu, X.; Zhou, Y.; Cao, Q.; Tu, J.; Wang, R.; et al. Underwater crack pixel-wise identification and quantification for dams via lightweight semantic segmentation and transfer learning. *Autom. Constr.* **2022**, *144*, 104600. [CrossRef]
9. Farzadnia, N.; Ali, A.A.A.; Demirboga, R. Characterization of high strength mortars with nano alumina at elevated temperatures. *Cem. Concr. Res.* **2013**, *54*, 43–54. [CrossRef]
10. Lu, J.-Q.; Wu, J.; Duan, W.; Liu, F.; Zhu, B.-F.; Gu, B.-L. Metal-to-semiconductor transition in squashed armchair carbon nanotubes. *Phys. Rev. Lett.* **2003**, *90*, 156601. [CrossRef] [PubMed]
11. Berra, M.; Carassiti, F.; Mangialardi, T.; Paolini, A.E.; Sebastiani, M. Effects of nanosilica addition on workability and compressive strength of Portland cement pastes. *Constr. Build. Mater.* **2012**, *35*, 666–675. [CrossRef]
12. She, W.; Du, Y.; Miao, C.; Liu, J.; Zhao, G.; Jiang, J.; Zhang, Y. Application of organic-and nanoparticle-modified foams in foamed concrete: Reinforcement and stabilization mechanisms. *Cem. Concr. Res.* **2018**, *106*, 12–22. [CrossRef]
13. Li, Y.; Bao, T.; Li, T.; Wang, R. A robust real-time method for identifying hydraulic tunnel structural defects using deep learning and computer vision. *Comput. Civ. Infrastruct. Eng.* **2023**, *38*, 1381–1399. [CrossRef]
14. Li, Y.; Bao, T.; Huang, X.; Wang, R.; Shu, X.; Xu, B.; Tu, J.; Zhou, Y.; Zhang, K. An integrated underwater structural multi-defects automatic identification and quantification framework for hydraulic tunnel via machine vision and deep learning. *Struct. Health Monit.* **2023**, *22*, 2360–2383. [CrossRef]
15. Li, Y.; Bao, T.; Gao, Z.; Shu, X.; Zhang, K.; Xie, L.; Zhang, Z. A new dam structural response estimation paradigm powered by deep learning and transfer learning techniques. *Struct. Health Monit.* **2021**, *21*, 770–787. [CrossRef]
16. Jo, B.-W.; Kim, C.-H.; Tae, G.; Park, J.-B. Characteristics of cement mortar with nano-SiO_2 particles. *Constr. Build. Mater.* **2007**, *21*, 1351–1355. [CrossRef]
17. Said, A.M.; Zeidan, M.S.; Bassuoni, M.T.; Tian, Y. Properties of concrete incorporating nano-silica. *Constr. Build. Mater.* **2012**, *36*, 838–844. [CrossRef]
18. Oltulu, M.; Şahin, R. Pore structure analysis of hardened cement mortars containing silica fume and different nano-powders. *Constr. Build. Mater.* **2014**, *53*, 658–664. [CrossRef]
19. Chen, Y.; Deng, Y.; Li, M. Influence of Nano-SiO_2 on the Consistency, Setting Time, Early-Age Strength, and Shrinkage of Composite Cement Pastes. *Adv. Mater. Sci. Eng.* **2016**, *2016*, 5283706. [CrossRef]
20. Bianchi, G.Q.; Brouwers, H.J.H. Application of nano-silica (nS) in concrete mixtures. In Proceedings of the 8th Fib International PhD Symposium in Civil Engineering, Copenhagen, Denmark, 20–23 June 2010; pp. 431–436.
21. Zhao, H.; Jiang, K.; Yang, R.; Tang, Y.; Liu, J. Experimental and theoretical analysis on coupled effect of hydration, temperature and humidity in early-age cement-based materials. *Int. J. Heat Mass Transf.* **2020**, *146*, 118784. [CrossRef]
22. Zhao, H.; Liu, J.; Yin, X.; Wang, Y.; Huang, D. A multiscale prediction model and simulation for autogenous shrinkage deformation of early-age cementitious materials. *Constr. Build. Mater.* **2019**, *215*, 482–493. [CrossRef]
23. Zhang, P.; Wittmann, F.H.; Vogel, M.; Müller, H.S.; Zhao, T. Influence of freeze-thaw cycles on capillary absorption and chloride penetration into concrete. *Cem. Concr. Res.* **2017**, *100*, 60–67. [CrossRef]
24. Wang, Q.; Yang, J.; Chen, H. Long-term properties of concrete containing limestone powder. *Mater. Struct.* **2017**, *50*, 168. [CrossRef]

25. Zhang, P.; Li, Q.; Wang, J.; Shi, Y.; Ling, Y. Effect of PVA fiber on durability of cementitious composite containing nano-SiO_2. *Nanotechnol. Rev.* **2019**, *8*, 116–127. [CrossRef]
26. Wang, Y.; Cao, Y.; Zhang, P.; Ma, Y.; Zhao, T.; Wang, H.; Zhang, Z. Water absorption and chloride diffusivity of concrete under the coupling effect of uniaxial compressive load and freeze–thaw cycles. *Constr. Build. Mater.* **2019**, *209*, 566–576. [CrossRef]
27. Zhao, H.; Wu, X.; Huang, Y.; Zhang, P.; Tian, Q.; Liu, J. Investigation of moisture transport in cement-based materials using low-field nuclear magnetic resonance imaging. *Mag. Concr. Res.* **2021**, *73*, 252–270. [CrossRef]
28. Li, J.H.; He, X.B.; Hu, S.W.; Jiang, J.H.; Zhao, H.T. Advancs in autogenous shrinkage and its regulation of modern concrete. *Hydro Sci. Eng.* **2023**, *2*, 150–161.
29. Shen, D.; Liu, X.; Li, Q.; Sun, L.; Wang, W. Early-age behavior and cracking resistance of high-strength concrete reinforced with Dramix 3D steel fiber. *Constr. Build. Mater.* **2019**, *196*, 307–316. [CrossRef]
30. Zhao, H.; Jiang, K.; Di, Y.; Xu, W.; Li, W.; Tian, Q.; Liu, J. Effects of curing temperature and superabsorbent polymers on hydration of early-age cement paste containing a CaO-based expansive additive. *Mater. Struct.* **2019**, *52*, 108. [CrossRef]
31. Zhutovsky, S.; Kovler, K. Effect of internal curing on durability-related properties of high performance concrete. *Cem. Concr. Res.* **2012**, *42*, 20–26. [CrossRef]
32. Cusson, D.; Hoogeveen, T. Internal curing of high-performance concrete with pre-soaked fine lightweight aggregate for prevention of autogenous shrinkage cracking. *Cem. Concr. Res.* **2008**, *38*, 757–765. [CrossRef]
33. Jensen, O.M.; Hansen, P.F. Water-entrained cement-based materials: I. Principles and theoretical background. *Cem. Concr. Res.* **2001**, *31*, 647–654. [CrossRef]
34. Craeye, B.; Geirnaert, M.; De Schutter, G. Super absorbing polymers as an internal curing agent for mitigation of early-age cracking of high-performance concrete bridge decks. *Constr. Build. Mater.* **2011**, *25*, 1–13. [CrossRef]
35. Qin, H.G.; Gao, M.R.; Pang, C.M.; Sun, W. Research on performance inprovement of expansive concrete with internal curing angent SAP and its action mechanism. Journal of building materials. *Hydro Sci. Eng.* **2011**, *14*, 394–399.
36. Shen, D.; Wang, X.; Cheng, D.; Zhang, J.; Jiang, G. Effect of internal curing with super absorbent polymers on autogenous shrinkage of concrete at early age. *Constr. Build. Mater.* **2016**, *106*, 512–522. [CrossRef]
37. Canul-Polanco, A.J.; Durán-Herrera, A.; Valdez-Tamez, P. Autogenous Shrinkage in High Performance Concrete with Chemical Admixtures. *Key Eng. Mater.* **2016**, *711*, 143–149. [CrossRef]
38. Mechtcherine, V.; Gorges, M.; Schroefl, C.; Assmann, A.; Brameshuber, W.; Ribeiro, A.B.; Cusson, D.; Custódio, J.; da Silva, E.F.; Ichimiya, K.; et al. Effect of internal curing by using superabsorbent polymers (SAP) on autogenous shrinkage and other properties of a high-performance fine-grained concrete: Results of a RILEM round-robin test. *Mater. Struct.* **2014**, *47*, 541–562. [CrossRef]
39. Justs, J.; Wyrzykowski, M.; Bajare, D.; Lura, P. Internal curing by superabsorbent polymers in ultra-high performance concrete. *Cem. Concr. Res.* **2015**, *76*, 82–90. [CrossRef]
40. *GB 175-2023*; Common Portland Cement. Chinese Standard Press: Beijing, China, 2023.
41. Snoeck, D.; Schröfl, C.; Mechtcherine, V. Recommendation of RILEM TC 260-RSC: Testing sorption by superabsorbent polymers (SAP) prior to implementation in cement-based materials. *Mater. Struct.* **2018**, *51*, 116. [CrossRef]
42. *ASTM C1761/C1761M-17*; Standard Specification for Lightweight Aggregate for Internal Curing of Concrete. ASTM: West Conshohocken, PA, USA, 2017.
43. Khaloo, A.; Mobini, M.H.; Hosseini, P. Influence of different types of nano-SiO_2 particles on properties of high-performance concrete. *Constr. Build. Mater.* **2016**, *113*, 188–201. [CrossRef]
44. *ASTM C192/C192M*; Standard Practice for Making and Curing Concrete Test Specimens in the Laboratory. ASTM: West Conshohocken, PA, USA, 2016.
45. Zhang, J.; Hou, D.; Han, Y. Micromechanical modeling on autogenous and drying shrinkages of concrete. *Constr. Build. Mater.* **2012**, *29*, 230–240. [CrossRef]
46. Concrete, I.J. Technical committee report on autogenous shrinkage. *Proc. JCI* **1998**, *795*, 1–63.
47. Amin, M.N.; Kim, J.-S.; Dat, T.T.; Kim, J.-K. Improving test methods to measure early age autogenous shrinkage in concrete based on air cooling. *IES J. Part A Civ. Struct. Eng.* **2010**, *3*, 244–256. [CrossRef]
48. Zhang, J.; Dongwei, H.; Wei, S. Experimental study on the relationship between shrinkage and interior humidity of concrete at early age. *Mag. Concr. Res.* **2010**, *62*, 191–199. [CrossRef]
49. Tian, Q.; Wang, Y.J.; Zhang, H.; Liu, J.; Miao, C. In-situ monitoring of setting of concrete based on pore water pressure measurement. In Proceedings of the Second International Conference on Microstructural-related Durability of Cementitious Composites, Amsterdam, the Netherlands, 11–13 April 2012.
50. Slowik, V.; Schmidt, M.; Fritzsch, R.; Jiang, J.H. Capillary Pressure in Fresh Cement-based Materials and Identification of the Air Entry Value. *Cem. Constr. Comp.* **2008**, *30*, 557–565. [CrossRef]
51. Leemann, A.; Nygaard, P.; Lura, P. Impact of Admixtures on the Plastic Shrinkage Cracking of Self-compacting Concrete. *Cem. Constr. Comp.* **2014**, *46*, 1–7. [CrossRef]

52. Zhang, J.L.; Tian, Q.; Wang, Y.J.; Li, M.; Wang, W.; Li, H.; Yao, T. Study on Testing Methods of Capillary Depression of Cement-based Materials. *Constr.* **2016**, *12*, 44–47.
53. *ASTM C39/C39M-20*; Standard Test Method for Compressive Strength of Cylindrical Concrete Samples, Vol. 9. ASTM International: West Conshohocken, PA, USA, 2020.
54. Zhao, H.; Qin, X.; Liu, J.; Zhou, L.; Tian, Q.; Wang, P. Pore structure characterization of early-age cement pastes blended with high-volume fly ash. *Constr. Build. Mater.* **2018**, *189*, 934–946. [CrossRef]
55. Kawashima, S.; Hou, P.; Corr, D.J.; Shah, S.P. Modification of cement-based materials with nanoparticles. *Cem. Concr. Compos.* **2013**, *36*, 8–15. [CrossRef]
56. Qing, Y.; Zenan, Z.; Deyu, K.; Rongshen, C. Influence of nano-SiO_2 addition on properties of hardened cement paste as compared with silica fume. *Constr. Build. Mater.* **2007**, *21*, 539–545. [CrossRef]
57. Zheng, L.; Xuehua, C.; Mingshu, T. Hydration and setting time of MgO-type expansive cement. *Cem. Concr. Res.* **1992**, *22*, 1–5. [CrossRef]
58. Ji, T.; Zheng, D.-D.; Chen, X.-F.; Lin, X.-J.; Wu, H.-C. Effect of prewetting degree of ceramsite on the early-age autogenous shrinkage of lightweight aggregate concrete. *Constr. Build. Mater.* **2015**, *98*, 102–111. [CrossRef]
59. Liu, K.; Yu, R.; Shui, Z.; Li, X.; Guo, C.; Yu, B.; Wu, S. Optimization of autogenous shrinkage and microstructure for Ultra-High Performance Concrete (UHPC) based on appropriate application of porous pumice. *Constr. Build. Mater.* **2019**, *214*, 369–381. [CrossRef]
60. Moosberg-Bustnes, H.; Lagerblad, B.; Forssberg, E. The function of fillers in concrete. *Mater. Struct.* **2004**, *37*, 74–81. [CrossRef]
61. Oey, T.; Kumar, A.; Bullard, J.W.; Neithalath, N.; Sant, G. The filler effect: The influence of filler content and surface area on cementitious reaction rates. *J. Am. Ceram. Soc.* **2013**, *96*, 1978–1990. [CrossRef]
62. Dai, X.Q.; Shen, A.Q.; Li, Z.N.; Yang, J.Y. Durability performance of superabsorbent polymer incorporated concrete modified by nano-silica addition in seasonal frozen regions. *Mater. Tod. Commun.* **2024**, *40*, 109727. [CrossRef]
63. Igarashi, S.; Watanabe, A.; Jensen, O.M.; Lura, P.; Kovler, K. Experimental study on prevention of autogenous deformation by internal curing using super-absorbent polymer particles. In Proceedings of the International RILEM Conference on Volume Changes of Hardening Concrete: Testing and Mitigation, Lyngby, Denmark, 20–23 August 2006; Volume 100, pp. 77–86.
64. Yang, J.; Wang, F.; Liu, Z.; Liu, Y.; Hu, S. Early-state water migration characteristics of superabsorbent polymers in cement pastes. *Cem. Concr. Res.* **2019**, *118*, 25–37. [CrossRef]
65. Wei, Y.; Hansen, W.; Biernacki, J.J.; Schlangen, E. Unified shrinkage model for concrete from autogenous shrinkage test on paste with and without ground-granulated blast-furnace slag. *ACI Mater. J.* **2011**, *108*, 13.
66. See, H.T.; Attiogbe, E.K.; Miltenberger, M.A. Potential for restrained shrinkage cracking of concrete and mortar. *Cem. Concr. Aggreg.* **2004**, *26*, 123–130. [CrossRef]

Disclaimer/Publisher's Note: The statements, opinions and data contained in all publications are solely those of the individual author(s) and contributor(s) and not of MDPI and/or the editor(s). MDPI and/or the editor(s) disclaim responsibility for any injury to people or property resulting from any ideas, methods, instructions or products referred to in the content.